pH-Dependent Fluorescence of $[La(OH)_2]^+[ARS]^-$ Hybrid Nanoparticles for Intracellular pH-Sensing

Kristina Sabljo,[a] Joanna Napp,[b,c] Frauke Alves,[b,c]* and Claus Feldmann[a]*

[a] Karlsruhe Institute of Technology (KIT), Institute for Inorganic Chemistry, Engesserstrasse 15, 76131 Karlsruhe, Germany. E-mail: claus.feldmann@kit.edu

[b] University Medical Center Goettingen (UMG), Institute for Diagnostic and Interventional Radiology, Robert Koch Str. 40, 37075 Goettingen, Germany

[c] Max Planck Institute for Multidisciplinary Sciences, Translational Molecular Imaging, Hermann-Rein-Strasse 3, 37075 Goettingen, Germany. E-mail: falves@gwdg.de

– Electronic Supporting Information (ESI) –

Content:

1. Analytical Methods

Dynamic Light Scattering (DLS) was used to determine the hydrodynamic diameter and size distribution of the $[La(OH)_2]^+[ARS]^-$ IOH-NPs in aqueous suspensions. For measurements, 1 mL of the aqueous $[La(OH)_2]^+[ARS]^-$ IOH-NP suspension containing 2 mg/mL of the IOH-NPs was diluted with 9 mL of demineralized water. Measurements were performed in polystyrene cuvettes applying a Nanosizer ZS (Malvern Instruments, United Kingdom) with backscattering geometry (173 °).

Zeta Potential Measurements were conducted using an automatic titrator MPT-2 attached to the aforementioned Nanosizer ZS (Malvern Instruments, United Kingdom). For measurements, 1 mL of the aqueous $[La(OH)_2]^+[ARS]^-$ IOH-NP suspension containing 2 mg/mL of the IOH-NPs was diluted with 9 mL of demineralized water. Titrations were performed using 0.1 M HCl and 0.1 M as well as 0.01 M NaOH.

Scanning electron microscopy (SEM) was carried out with a Zeiss Supra 40 VP (Zeiss, Germany) with a field emission gun (acceleration voltage 1 kV, working distance 3 mm). $[La(OH)_2]^+[ARS]^-$ IOH-NP samples were prepared by depositing a droplet of a diluted aqueous suspension on a silicon wafer.

Energy-dispersive X-ray spectroscopy (EDXS) was performed with an Ametec EDAX device (Ametec, USA) mounted on a Zeiss SEM Supra 35 VP scanning electron microscope. For this purpose, the $[La(OH)_2]^+[ARS]^-$ IOH-NPs were pressed to dense pellets and fixed with conductive carbon pads on aluminium sample holders. EDXS was only used to validate the presence of lanthanum and sulphur in the IOH-NPs.

Fourier-transformed infrared (FT-IR) spectra were recorded with a Bruker Vertex 70 FT-IR spectrometer (Bruker, Germany) in the range 4000-400 cm^{-1} with a resolution of 4 cm^{-1}. 1 mg of the dried $[La(OH)_2]^+[ARS]^-$ IOH-NP sample was pestled with 300 mg of KBr and pressed to a pellet.

X-ray powder diffraction (XRD) measurements were conducted with a STADI-P diffractometer (Stoe, Germany) with Ge-monochromatized Cu-K_α-radiation (λ = 1.54278 Å) and Debye-Scherrer geometry. Sample for measurements in transmission were placed on sodium acetate foils and fixed with an amorphous adhesive film.

Differential thermal analysis/thermogravimetry (DTA/TG) was performed with a STA409C device (Netzsch, Germany). The vacuum-dried $[La(OH)_2]^+[ARS]^-$ IOH-NPs (15-20 mg in corundum crucibles) were heated to 1200 °C with a rate of 1 K/min in air.

Elemental analysis (EA, C/H/N/S analysis) was performed via thermal combustion with an Elementar Vario Micro Cube (Elementar, Germany) at a temperature of 1100 °C.

Fluorescence spectroscopy (FL). Excitation and emission spectra were recorded with a resolution of ±1 nm using a photoluminescence spectrometer Spex Fluorolog 3 (Horiba Jobin Yvon, France), equipped with a 450 W Xe-lamp and double monochromators.

Ultraviolet-visible (UV-Vis) spectra were recorded on an UV 2700 spectrometer (Shimadzu, Japan) equipped with an Ulbricht sphere.

pH measurements. pH values of aqueous solutions and suspensions were adjusted by addition of 0.01 M or 0.1 M HCl as well as 0.01 M or 0.1 M NaOH. The pH values were measured with a significance of ±0.01, using a pH meter HI2211 pH/ORP (Hanna Instruments, Germany).

2. Experimental

$[La(OH)_2]^+[ARS]^-$ IOH-NPs were prepared by dissolving 36.0 mg (0.1 mmol) of alizarin red S sodium salt (Na(ARS), Riedel-de Haën, indicator grade) in 50 mL of demineralized water. Thereafter, 0.5 mL of an aqueous solution containing (0.09 mmol) of $LaCl_3 \cdot 7H_2O$ (Sigma Aldrich, 99.9%) were injected, which results in an instantaneous nucleation of nanoparticles. After 2 min of intense stirring, the as-prepared IOH-NPs were separated via centrifugation (25.000 rpm, 15 min) and twice purified by redispersion/centrifugation in/from H_2O. For analytical characterization, the dark violet $[La(OH)_2]^+[ARS]^-$ IOH-NPs were redispersed in demineralized water or dried to powder samples.

3. pH-dependent Behaviour of Na(ARS)

For comparison with the $[La(OH)_2]^+[ARS]^-$ IOH-NPs, the pH-dependent properties of the freely dissolved pH indicator ARS (Na(ARS)) was examined (Figure S1). In solution, the colour at different pH values turned from yellow (pH = 2.5-4.5) via pale orange (pH = 5.5-9.0) to pink (pH > 9.0) (Figure S1a). This colour change is in agreement with the pK_a value of 5.5.[S1] Two distinct regions of absorption were observed with maxima at 520 nm (pH = 5.5-9.0) and 420 nm (pH < 5.5) (*see main paper: Figure 3a*).

Depending on the pH, ARS occurs with three different molecular forms with only the anionic SO_3^- group (pH < 4.5), an additional deprotonated OH group (pH 4.5-9.0) or even two deprotonated OH groups (pH > 9.5) (Figure S1b). For theses molecular forms, fluorescence spectroscopy indicates broad excitation at 425-475 nm in a pH range of 5.5-9.0. In comparison, excitation spectra at strongly acidic pH (<4.5) exhibit only less specific and low-intensity features (Figure S1c). At pH levels of 5.5-9.0, emission at 500-650 nm (λ_{exc}: 462 nm) was observed (Figure S1d). For lower pH levels (pH < 4.5), the emission shifts to even longer wavelengths.

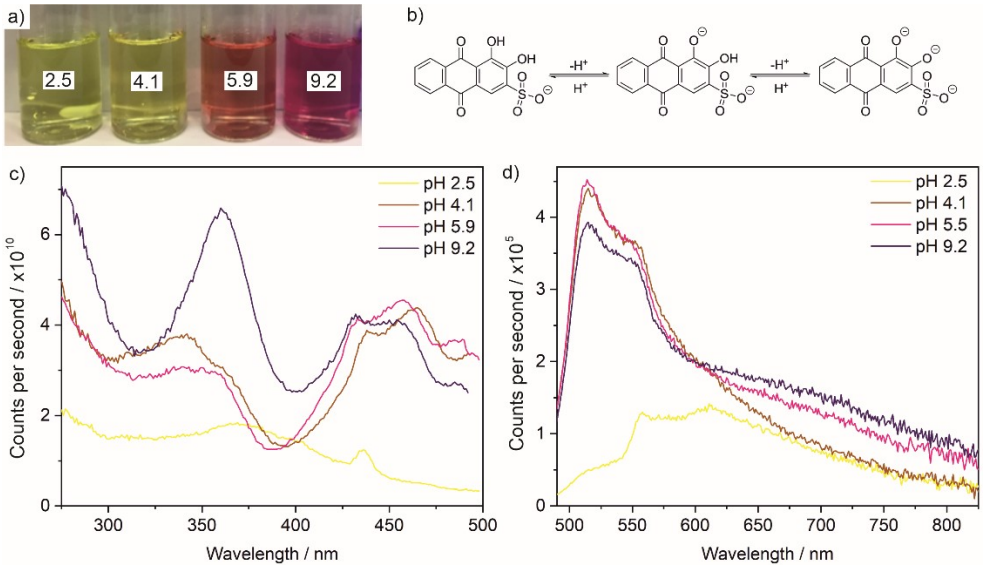

Figure S1. pH-dependent optical properties of freely dissolved ARS: (a) Photos of aqueous ARS solutions at different pH values; (b) pH-dependent molecular structure of ARS; (c) Excitation spectra (λ_{em}: 512 nm), and (d) emission spectra (λ_{exc}: 462 nm) at different pH levels.

4. Material Characterization of $[La(OH)_2]^+[ARS]^-$ IOH-NPs

The range of interest for intracellular measurements is between 4.5 and 7.4, which includes pH variations in the cytosol (pH 6.8-7.4) and in cellular compartments such as endosomes (pH 4.4-6.0) and lysosomes (pH 4.5-5.0).[S2] Therefore, the stability and particle size of the $[La(OH)_2]^+[ARS]^-$ IOH-NPs were examined in this pH range. According the DLS analysis at different pH values, the particle size remains stable in a pH range of 4-8 (Figure S2). At strongly acidic (pH < 4) or basic (pH > 8), particle size and particle stability decrease, which indicates beginning particle dissolution.

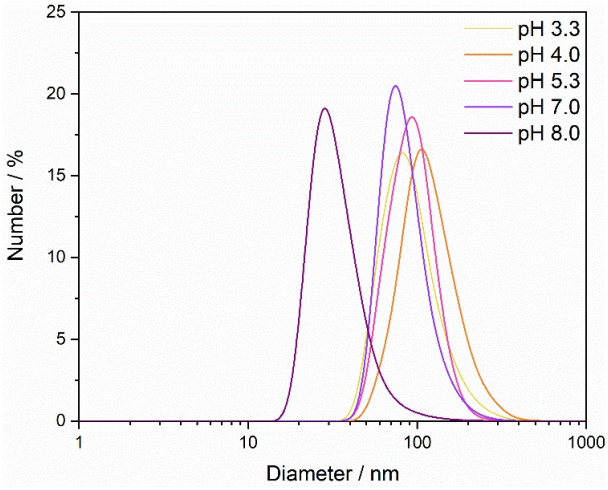

Figure S2. Particle size of aqueous suspensions depending on the pH (according to DLS).

In addition to the pH-dependent fluorescence of the $[La(OH)_2]^+[ARS]^-$ IOH-NPs, the influence of the pH on the particle size and particle shape was examined (Figure S3). Similar to the DLS data, the size and shape of the $[La(OH)_2]^+[ARS]^-$ IOH-NPs remained unaffected in a pH range of 4-8, whereas the IOH-NPs become smaller and more agglomerated at lower and higher pH, which indicates beginning dissolution and decreasing colloidal stability.

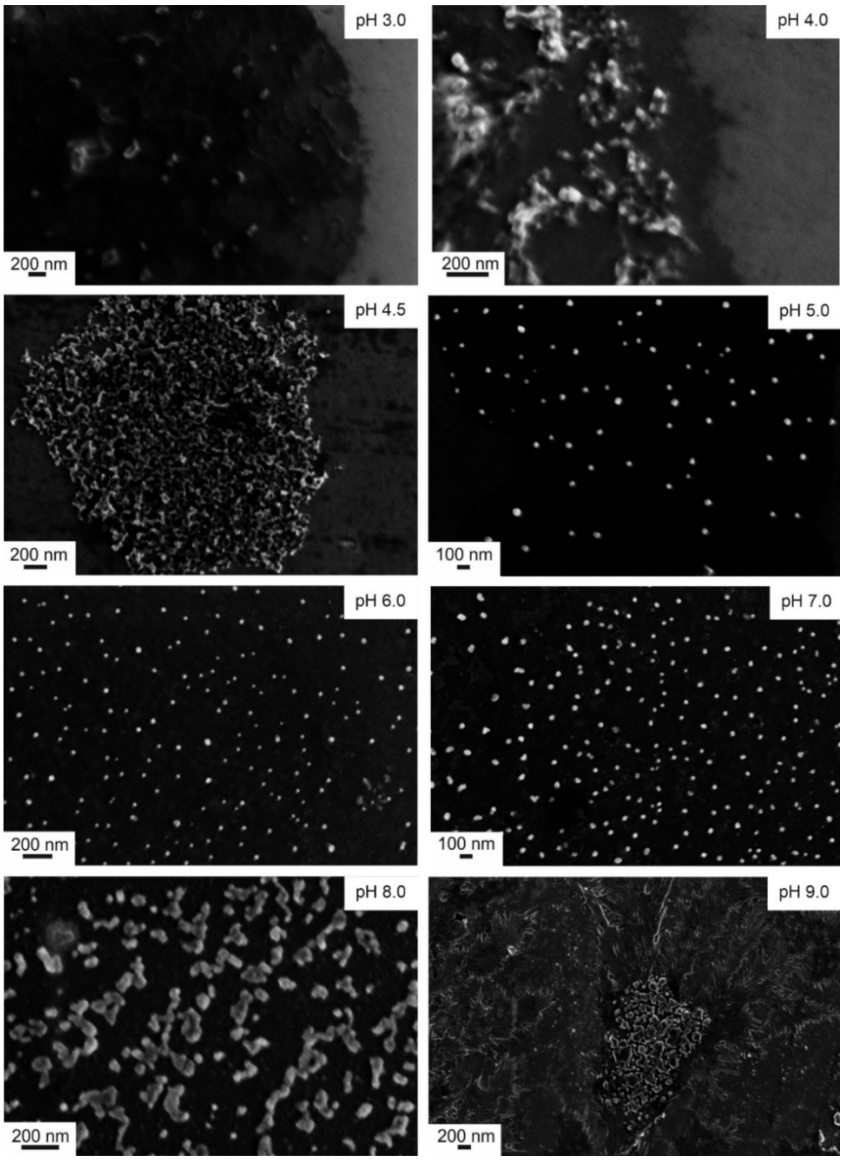

Figure S3. pH-depending particle size and shape of the $[La(OH)_2]^+[ARS]^-$ IOH-NPs in a pH range of 3.0 to 9.0.

To prove the chemical composition of the $[La(OH)_2]^+[ARS]^-$ IOH-NPs, different analytical methods were used. First of all, X-ray diffraction (XRD) indicates the IOH-NPs to be non-crystalline (Figure S4). In regard of the large size of the $[ARS]^-$ anion, this finding is not a surprise and has frequently been observed for other IOH-NPs.[S3,S4] Fourier-transformed infrared (FT-IR) spectroscopy evidences the presence of ARS (Figure S5a). Accordingly, spectra of $[La(OH)_2]^+[ARS]^-$ are well in agreement with the starting material and show the characteristic ARS-type vibrations, including ν(Ar–C=O): 1700-1600 cm^{-1}, ν(Ar–C=C): 1590 cm^{-1}, ν(Ar–C–O): 1260 cm^{-1}, $\nu_{as}(SO_3)$: 1200-1100 cm^{-1}, $\nu_s(SO_3)$: 1100-950 cm^{-1}, and ν(Ar–C–H): 950-600 cm^{-1}.[S5] Furthermore, ν(O–H) at 3600-3000 cm^{-1} indicates the presence of water. Energy

dispersive X-ray spectroscopy (EDXS) confirms the presence of lanthanum and sulphur in the IOH-NPs (Figure S6).

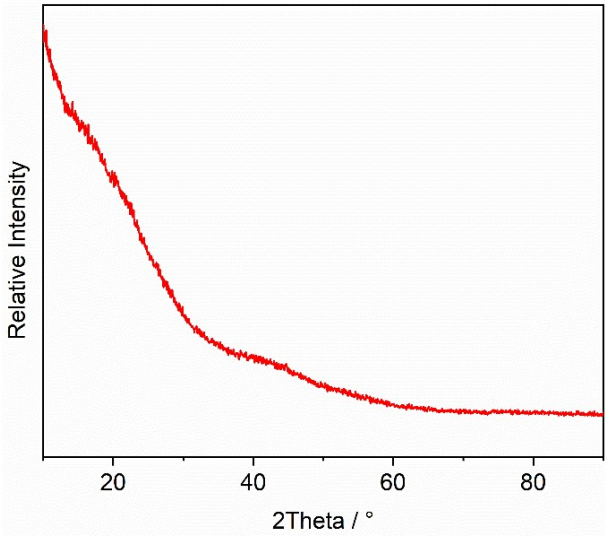

Figure S4. XRD of the as-prepared $[La(OH)_2]^+[ARS]^-$ IOH-NPs.

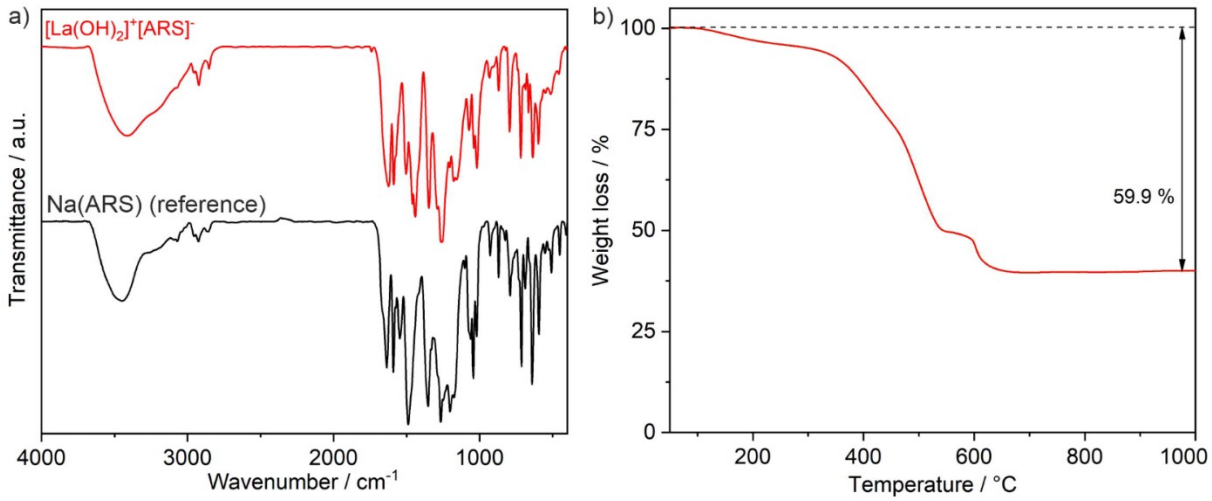

Figure S5. Chemical composition of the as-prepared $[La(OH)_2]^+[ARS]^-$ IOH-NPs: (a) FT-IR spectrum (Na(ARS) as a reference); (b) Thermogravimetric analysis.

To quantify the chemical composition of the $[La(OH)_2]^+[ARS]^-$ IOH-NPs, elemental analysis (EA) and thermogravimetry (TG) were applied. Prior to the thermal combustion analyses, the as-prepared IOH-NPs were dried in vacuum at room temperature for 8 h to remove all adsorbed water. EA results in 34.1 wt-% C, 2.7 wt-% H, and 6.1 wt-% S, which fits well with calculated values of $[La(OH)_2]^+[ARS]^-$ (34.2 wt-% C, 1.8 wt-% H, 6.5 wt-% S). TG shows a total organics loss of 59.9% up to a temperature of 600 °C (Figure S5b). The thermal residue of 41.1% was identified by XRD to be $La_2O_2(SO_4)$ (Figure S7). Again, these values

agree with the composition $[La(OH)_2]^+[ARS]^-$ with a calculated mass loss of 59.5%. In sum, the thermal combustion can be rationalized as follows: $2[La(OH)_2]^+[C_{14}H_7O_7S]^- + 27.5O_2 \rightarrow La_2O_2(SO_4) + 28CO_2 + 9H_2O + SO_2$. Taken together, FT-IR, EDXS, EA, and TG confirm the composition $[La(OH)_2]^+[ARS]^-$ with 65 wt-% ARS of total IOH-NP mass.

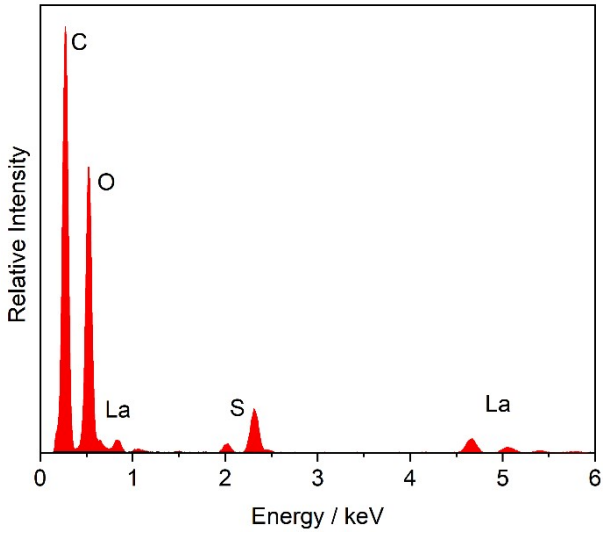

Figure S6. EDXS of the as-prepared $[La(OH)_2]^+[ARS]^-$ IOH-NPs.

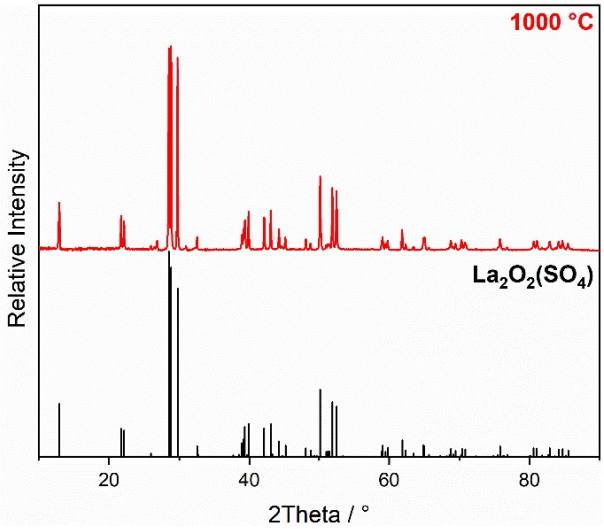

Figure S7. XRD of the thermal remnant of the $[La(OH)_2]^+[ARS]^-$ IOH-NPs subsequent to the TG analysis ($La_2O_2(SO_4)$ as a reference: ICDD-No. 01-085-1535).

5. In-vitro Studies

Cell cultures. The immortalized and adherent mouse alveolar macrophage cell line, MH-S (CRL-2019, ATCC) was cultivated at 37 °C in a humidified atmosphere of 5% CO_2 in complete RPMI medium supplemented with 10% fetal calf serum (FCS) and 0.05 mM 2-mercaptoethanol.

Incubation with IOH-NPs. MH-S cells were plated on a 35 mm µ-dish equipped with a polymer coverslip bottom (IBIDI), in a concentration of ~15.000 cells/cm² in 1 mL cell culture medium. Cells were allowed to attach overnight. On the next day, the macrophages were supplemented with 1 mL of medium, containing 50 µg/mL of the $[La(OH)_2]^+[ARS]^-$ IOH-NPs and 1 µL/mL DAPI for nuclear counterstain.

Microscopy and image analysis. A Leica SP5 confocal laser-scanning microscope was used for imaging. Time-resolved live cell imaging was performed after 30 min and 5 h of incubation with the IOH-NPs. $[La(OH)_2]^+[ARS]^-$ IOH-NPs were excited at 458 nm, and the emission recorded at 500-550, 550-650, and 650-750 nm (*see main paper: Figure 5b*). DAPI was excited at 405 nm and the emission recorded at 410-460 nm. Imaging of fixed and antibody-stained cells was performed using excitation of IOH-NPs at 488 nm, and emission recorded at 550-650 nm, and Alexa Fluor 633 using excitation at 633 nm, and emission recorded at 650-800 nm (*see main paper: Figure 6*). DAPI was excited at 405 nm and the emission recorded at 420-450 nm. Confocal images were processed using ImageJ (available by ftp at *zippy.nimh.nih.gov* or at *http://rsb.info.nih.gov/nih-imageJ,* developed by W. Rasband, National Institutes of Health, U.S.).

The toxicity of the $[La(OH)_2]^+[ARS]^-$ IOH-NPs was examined by MTT assays and compared to solutions of Na(ARS) as a reference (Figure S8). Accordingly, the $[La(OH)_2]^+[ARS]^-$ IOH-NPs do not show any relevant toxicity up to high concentrations of 50 µg/mL. Neither the addition of $[La(OH)_2]^+[ARS]^-$ nor the addition of the freely dissolved ARS affected the growth of the cultured macrophages on a timescale of up to 72 hours.

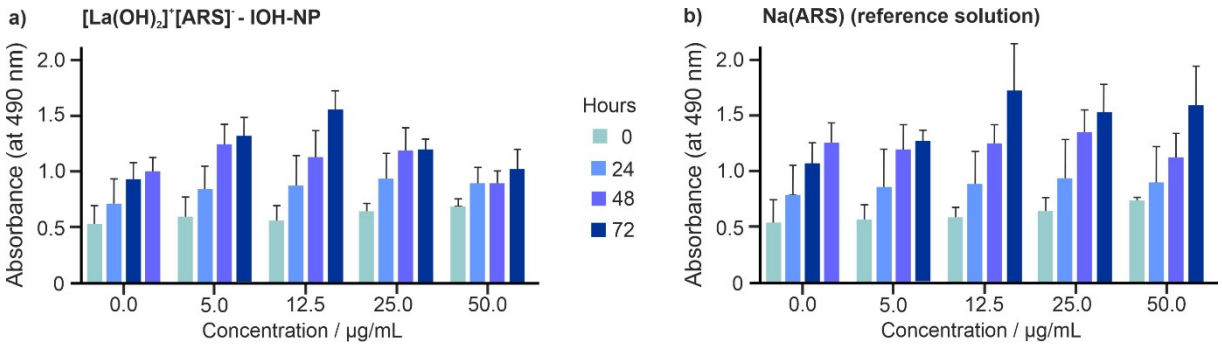

Figure S8. MTT assay indicating low systemic toxicity of the $[La(OH)_2]^+[ARS]^-$ IOH-NPs (a) with Na(ARS) solution as a reference (b).

Antibody staining. Staining with antibodies directed against different intracellular compartments was performed on fixed MH-S cells to co-localize the IOH-NPs. To this concern, MH-S cells were plated on 12 mm glass coverslips, coated with poly-L-lysine, inserted in 24 well plates in a concentration of ~50.000 cells/well. Cells were allowed to attach overnight. On the next day, the macrophages were incubated with 50 µg/mL of the $[La(OH)_2]^+[ARS]^-$ IOH-NPs for 30 min, 5 h, and 24 h. Cells were washed twice with PBS, fixed with 4% paraformaldehyde for 15 min and stored in PBS/0.04% sodium azide at 4 °C. After permeabilization of the cells with 0.1% Triton X 100 in PBS for 35 min and blocking with Seablock at room temperature (RT) for 1 h, the coverslips with cells were incubated with either rabbit-anti-mouse Rab7, 1 : 100 (PA5-52369) or rabbit-anti-mouse Rab11, 1 : 100 (700184) (both from Thermo Fisher) for 2 h at RT and overnight at 4 °C. After washing the following fluorescently labeled secondary antibody (Invitrogen) was applied for 2 h at RT in a dilution of 1 : 200 with Goat-anti-rabbit Alexa 633 (21071). After several washing steps with PBS with 0.05% Tween, cell nuclei were counterstained for 15 min at RT with Hoechst 33342 (dilution 1 : 500 in PBS with 0.05% Tween). Coverslips were mounted with Immu-Mount (Fisher Scientific).

In contrast to the antibody staining with Rab7 (*see main paper: Figure 6*), the $[La(OH)_2]^+[ARS]^-$ IOH-NPs do not co-localize with Rab11, which is associated with recycling endosomes (Figure S9*)*.

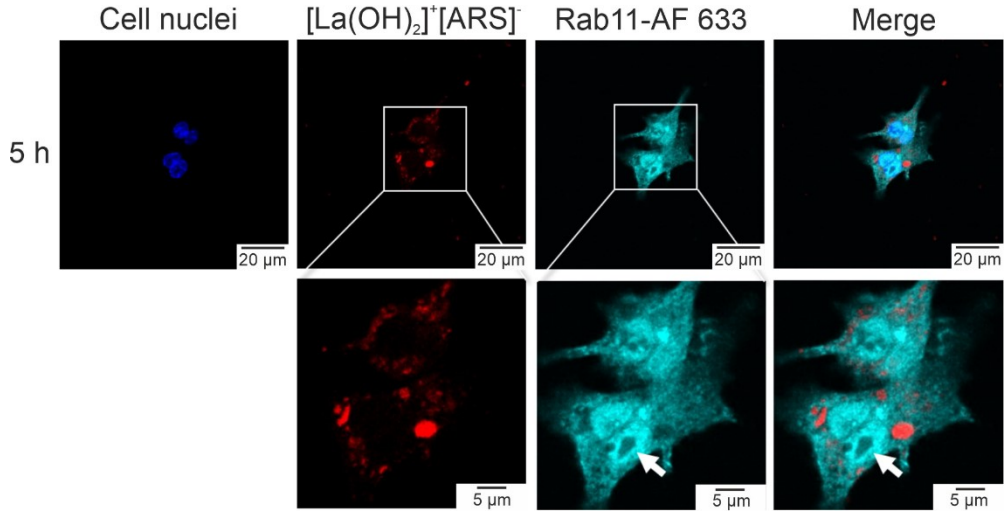

Figure S9. $[La(OH)_2]^+[ARS]^-$ IOH-NPs do not co-localize with recycling endosomes: MH-S cells were incubated with the IOH-NPs for 5 h and then fixed. Staining was performed with an anti-Rab11-antibody followed by the Alexa Flour 633 (AF 633) conjugated secondary antibody (cyan blue). Nuclei were labeled with Hoechst 33342 (dark blue). Second panel shows magnifications of the selected ROIs shown in the first panel. Right panels show merged images.

References

(S1) A. A. Shalaby and A. A. Mohamed, *RSC Adv.*, 2020, **10**, 11311-11316.

(S2) M. Schäferling, *WIREs Nanomed. Nanobiotechnol.*, 2016, **8**, 378-413.

(S3) (a) J. G. Heck, J. Napp, S. Simonato, J. Möllmer, M. Lange, H. R. Reichardt, R. Staudt, F. Alves and C. Feldmann, *J. Am. Chem. Soc.*, 2015, **137**, 7329-7336. (b) B. L. Neumeier, M. Khorenko, F. Alves, O. Goldmann, J. Napp, U. Schepers, H. M. Reichard and C. Feldmann, *ChemNanoMat.*, 2019, **5**, 24-45.

(S4) (a) M. Poß, E. Zittel, A. Meschkov, U. Schepers and C. Feldmann, *Bioconj. Chem.*, 2018, **29**, 2818-2828. (b) J. Napp, M. A. Markus, J. G. Heck, C. Dullin, W. Möbius, D. Gorpas, C. Feldmann and F. Alves, *Theranost.*, 2018, **8**, 6367-6368. (c) M. Poß, R. J. Tower, J. Napp, L. C. Appold, T. Lammers, F. Alves, C.-C. Glüer, S. Boretius and C. Feldmann, *Chem. Mater.*, 2017, **29**, 3547-3554.

(S5) O. A. Weisz, *Traffic,* 2003, **4**, 57-64.